ACS MEASUREMENT SCIENCE Au
AN OPEN ACCESS JOURNAL OF THE AMERICAN CHEMICAL SOCIETY

pubs.acs.org/measureau

Article

Reduction of the Measurement Time of a Chemiresistive Gas Sensor Using Transient Analysis and the Cantor Pairing Function

Srinivasulu Kanaparthi and Shiv Govind Singh*

Cite This: *ACS Meas. Sci. Au* 2022, 2, 113–119

Read Online

ACCESS | Metrics & More | Article Recommendations | Supporting Information

ABSTRACT: It is vital to measure the concentration of gas quickly in many gas sensing applications. Predicting the steady-state response from the earlier transient response is the economical and viable solution in this regard. However, existing transient analysis approaches either need huge data and computationally intensive algorithms or are inefficient. Here, we described a method to reduce the measurement time of the concentration of CH_4 with a chemiresistive gas sensor at room temperature (27 °C). The presented method considers the sensor's response at two fixed time intervals after gas exposure and maps their pairing number to the gas concentration. The proposed method measures the gas concentration in just 30 s from the gas exposure time. As the proposed method can quickly measure gas concentrations, it can be employed in widespread applications where quick quantification of gas is necessary.

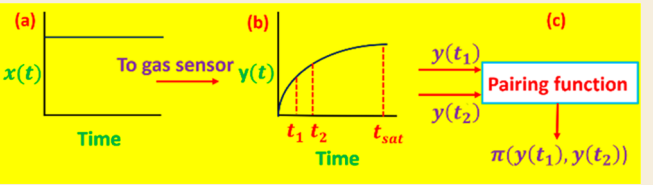

KEYWORDS: *measurement time reduction, reduction of response time, rapid gas sensing, ZnO gas sensor, chemiresistive gas sensor*

1. INTRODUCTION

Chemical gas sensors that transform chemical information to electrical signals have a strong demand in many applications, including environmental monitoring, healthcare, personal safety, and food quality analysis.[1−4] Numerous efforts have been made in the recent past to improve the sensitivity, selectivity, and limit of detection and reduce the energy consumption of the gas sensors by developing various material synthesis, device fabrication, and analytical strategies.[5−8] However, many applications also demand low measurement times to obtain sensing results. For example, it is crucial to instantly detect toxic or flammable gas leakage to avoid or minimize the loss of lives. The low measurement times in point-of-care applications facilitate more tests in a short duration and enhance the user experience. The use of low measurement time chemical sensors for food quality analysis allows the customers to know the dynamic expiry time of perishable products through electrical signals. In addition, the low measurement times eliminate the time-varying relative humidity (RH) induced errors in the sensor's response measurement. If the measurement time is high and the RH levels vary in this period, the sensor's steady-state response may not be the intended value as the variation in coadsorption of water molecules' density during the measurement affects the adsorption of the target gas. On the other hand, if the measurement time is low, RH might be at constant levels, and it does not affect the adsorption of gas molecules on the sensing layer.

There have been several materials-based studies on reducing measurement time, but they involve complex material synthesis or device fabrication strategies.[9,10] On the other hand, signal processing techniques are more economical and effective in reducing the measurement time of the sensors. Also, they are independent of materials and device structures and can be used in conjunction with other methods mentioned above. A few techniques have been proposed to reduce a sensor's measurement time using the transient response based on the curve fitting method, low pass derivative filter method, and neural networks.[11−18] The curve fitting can reduce the measurement time by only 45%, whereas neural networks are computationally intensive algorithms and require massive training data. The response derivative method and temporal response methods are simple and effective in measuring the concentration of the gases by correlating the signal peak with the gas concentration. However, derivative methods need higher sampling periods and high measurement times to get the apparent peak in slowly varying signals. Thus, it is necessary to find an approach that rapidly measures the sensor's response at low computational intensity.

In the current study, we presented a method for reducing the measurement time of a chemiresistive gas sensor operating at room temperature (27 °C) using transient response and the Cantor pairing function. The method was demonstrated by measuring the transient response of the graphene processed ZnO nanoflake (GZnO) sensor upon exposure to methane

Received: September 27, 2021
Revised: October 17, 2021
Accepted: October 19, 2021
Published: October 27, 2021

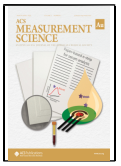

https://doi.org/10.1021/acsmeasuresciau.1c00043
ACS Meas. Sci. Au 2022, 2, 113–119

(CH_4) in the range of 25−100 ppm. In this approach, we measured the sensor's responses at two different intervals after the gas exposure and mapped them to a unique pairing number using the Cantor pairing function. The pairing number derived from the transient response exhibited a power-law relationship with the gas concentration, and thus, the gas concentration can be quantified from the transient response. The proposed method achieved a short and fixed measurement time of 30 s irrespective of the gas concentration. As the demonstrated method does not need any other data processing algorithms, it is a computationally less intensive method.

2. EXPERIMENTAL SECTION

Synthesis of GznO

GZnO is produced using a two-step chemical synthesis process. First, the ZnO nanostructures were synthesized with a wet chemical method.[8] Briefly, 0.1 M $Zn(CH_3COO)_2{\cdot}2H_2O$ and 0.5 M NaOH are dissolved in 30 mL of DI water and stirred at 50 °C for 40 min. Later, the solution is washed several times with ethanol and water, followed by drying at 60 °C to get white ZnO powder. In the second stage, ZnO is processed with graphene by mixing 3 mg of graphene with 30 mg of ZnO in 2 mL of ethylene glycol under ultrasonication for 2 h to get GZnO dissolved in ethylene glycol.

Materials Characterization

The crystal phase of the synthesized material is investigated using powder X-ray diffraction (XRD; PANalytical X'pert Pro) with Cu $K\alpha_1$ (λ = 1.5406 Å) in the 2θ range of 20−70°. The pore volume distribution of the material is investigated using a BET analyzer (MicroMeritics ASAP2020). Field-emission scanning electron microscopy (FESEM, JEOL JSM 7800F) is used to study the morphology of the synthesized samples.

Device Fabrication and Characterization

As described in our previous report, the GZnO pellets are prepared by applying high pressure on the powder material using a hydraulic press.[19] The patterning of sensing layers on paper followed by deposition of electrodes produced the sensor.[20,21] The patterning of sensing layers involves four steps: (i) designing the pattern, (ii) printing the toner patterns on paper, (iii) depositing sensing materials on the patterns, and (iv) removal of the toner on paper (Figure 1).

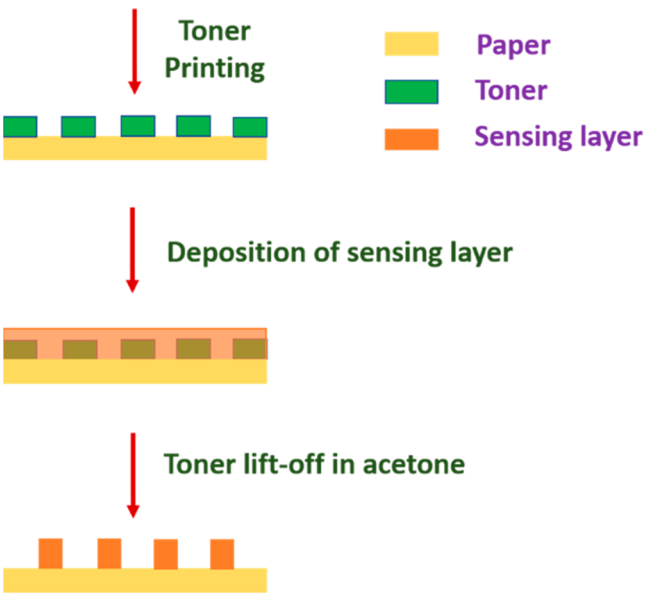

Figure 1. Patterning of a sensing layer on paper with printed toner lithography.

The required patterns are designed in PowerPoint so that the portion where the sensing films are to be deposited is kept blank and the remaining portion is dark. The designed patterns are printed on paper using a laser printer. The GZnO pellet was mechanically rubbed on the toner-printed paper in the next step. Finally, the toner is removed using acetone to get the required patterns of sensing layers. The silver paste is deposited as electrodes on both ends of the sensing films to finish the fabrication of the chemiresistive gas sensor. The surface roughness of sensors is characterized by Zeta 3D profilometry.

Gas Sensing Experiment

The sensor was characterized with the target gases using a customized gas sensing setup shown in Figure S1. It consists of a gas sensing chamber with electrical probes interfaced with the Keithley source measurement unit (SMU) to measure the sensor current. The gas cylinders are connected to the chamber through the manifold, and the gas composition is controlled using mass flow controllers (MFCs). The exposure gas composition is controlled by varying the flow rate of the reference gas and target gas by keeping the total flow rate constant. First, the sensor's current was stabilized in the reference gas and then exposed to the target gas's specified concentration. Once the sensor's current saturates under the target gas atmosphere, the target gas is replaced with the reference gas, and this process continues for all the concentrations of the target gases. The controlling of MFCs and the data acquisition through Keithley were performed using LabView-based software. It also controls solenoid valves, bias voltage, and the temperature and pressure of the sensing chamber. The data acquired from the sensor through Keithley is stored in an Excel file that contains the time, bias voltage, and sensor current. The gas humidity is controlled by using a bubbler filled with water through which a portion of the reference gas is passed. To achieve step input, we directly flow the gas on the sensor by replacing the reference gas with the target gas of specified concentration diluted in synthetic air.

3. RESULTS AND DISCUSSION

The crystal phases of the synthesized materials are investigated with X-ray diffraction (XRD) spectroscopy. The XRD peaks of ZnO and GZnO corresponding to (100), (002), and (101) planes in Figure 2a depict the wurtzite structure of ZnO (JCPDS 36-1451).[8] The peaks of GZnO are weaker in magnitude compared to those of pure ZnO. It suggests that the addition of graphene to ZnO influences the crystallinity of the material. However, no peak of graphene was observed in GZnO, which might be attributed to the low graphene concentration in GZnO.[22] The porosity of the material and the surface area of GZnO are investigated with BET analyzer. The sharp increase in the N_2 adsorption−desorption isotherm in Figure 2b at a relative pressure (P/P_0) > 0.8 indicates the presence of mesopores with a 5−50 nm diameter.[23] The surface area of GZnO determined with the BET surface area analyzer is 69.6 $m^2\ g^{-1}$. The mesoporous nature and high surface area of GZnO are driving factors for detecting the target gas with high sensitivity.

Further, the morphological characteristics of the material are observed using FESEM (Figure 3a). GZnO has 2D nanoflake structures and subsequently has a more active surface area for interaction of the target gas. The step size of the solid-state printed patterns is characterized by 3D optical profilometry. The profilometric images in Figure 3b show the step size of GZnO films printed on paper. As expected, the surface roughness is more, which is evident in hand-drawn films on paper. However, higher surface roughness is a positive factor, as the surface area available for gas molecules adsorption is more in rough surfaces than smooth surfaces. The higher surface area of the sensing layer enhances the device's sensitivity upon exposure to the target gases.

https://doi.org/10.1021/acsmeasuresciau.1c00043
ACS Meas. Sci. Au 2022, 2, 113−119

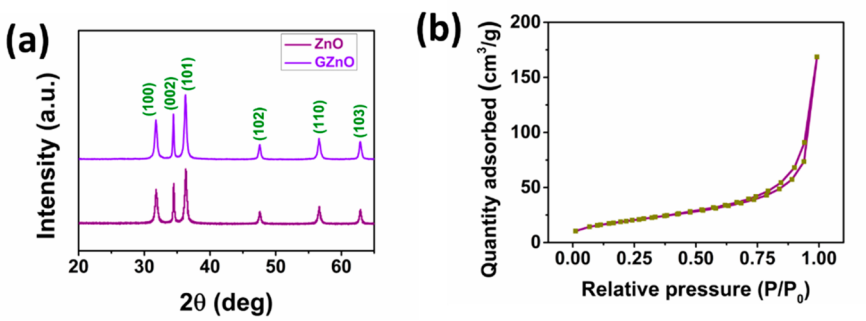

Figure 2. (a) XRD spectra of ZnO and GZnO and (b) N_2 adsorption−desorption curve.

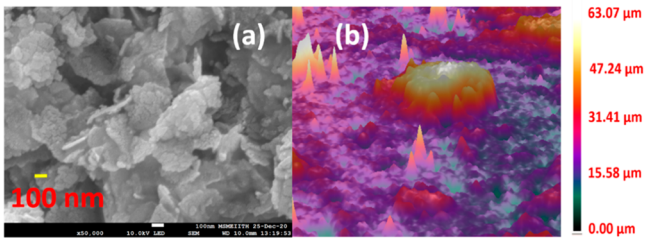

Figure 3. (a) FESEM image of GZnO and (b) 3D profilometry of GZnO deposited on the paper.

Before investigating the sensor's performance with CH_4, the thickness of the sensor was optimized for better performance. Figure S2 shows the sensor's response as a function of thickness upon exposure of 100 ppm of CH_4. The response decreases with the increase in thickness of the sensor from 10 to 25 μm. However, the resistance is too low when the thickness is below 15 μm. Therefore, 15 μm was chosen as the optimum thickness for the experiment. The optimized sensor is exposed to different concentrations of CH_4 gas at room temperature (27 °C, 50% RH) to demonstrate the patterns obtained with solid-state lithography. Figure 4a depicts the resistance of the sensor upon exposure CH_4. The resistance of the sensor decreases upon exposure to the target gas. It can be attributed to the electronic donating nature of CH_4 to n-type ZnO, which increases the sensor's conductivity upon exposure to the target gas. The steady-state response of 3 sensors is measured, and their average is plotted as shown in Figure 4b to

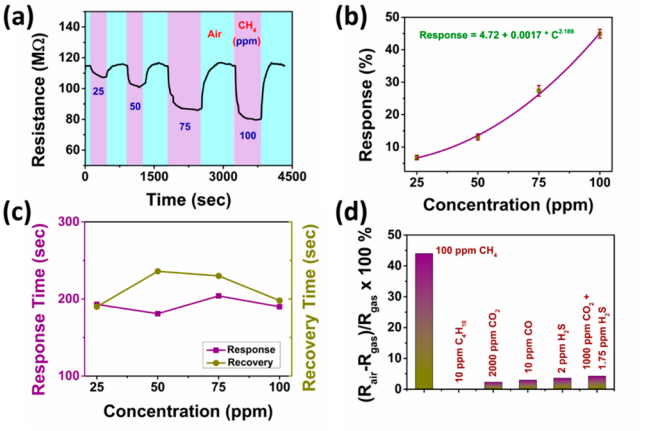

Figure 4. (a) Resistance of the sensor upon exposure to CH_4, (b) steady-state response of the sensor, (c) response and recovery times of the sensor, and (d) selectivity of the sensor to different target gases.

quantify the sensors's response as a function of the concentration of the target gases. The response (S) of the sensor has a power-law relation with the concentration (C) of the target gas as in (1).

$$S = 4.72 + 0.0017C^{2.189} \tag{1}$$

The response and recovery times are measured from the transient response and plotted in Figure 4c. The sensor's response time ranges from 191 to 204 s, whereas recovery is achieved within 190−236 s. It can be observed that the variation in response time with the concentration is insignificant and can be considered as constant with a slight standard deviation. The response time (t_r) of a reversible gas sensor can be represented with (2)

$$t_r = \frac{1}{k}\left(\frac{K}{1 + P_g K}\right) \tag{2}$$

where k, K, and P_g are the forward rate constant, reverse rate constant, and partial pressure of the target gas, respectively. The partial pressure of the gas is directly proportional to the concentration of the gas. At low concentrations of the target gas, (2) can be rewritten as (3)[24]

$$t_{r\lim P_g \to 0} = \lim P_g \to 0^{\left(\frac{1}{k}\right)*\left(\frac{K}{1+P_g K}\right)} = \frac{K}{k}\ (\text{constant}) \tag{3}$$

Thus, the sensor's response time is independent of gas concentration.

Further, the sensor's selectivity to the methane gas is investigated by exposing it to the other interference gases. We tested the sensor's response upon exposure to 10 ppm butane (C_4H_{10}), 2000 ppm of CO_2, 2 ppm of H_2S, and binary composition of 1000 ppm of CO_2 + 1.75 ppm of H_2S. All these concentrations are very high compared to the actual concentrations that exist in the air. It can be observed that the sensor's response to all the interfering gases is negligible compared to that of methane, as shown in Figure 4d, and it depicts the selective behavior of the sensor to the CH_4 in specific applications like natural gas leakage detection.

The detailed gas sensing mechanism of GZnO is outlined in Figure 5. The local heterojunctions formed between graphene and ZnO are responsible for the sensor's high sensitivity to the target gas.[25] As the work function of ZnO is relatively smaller than that of graphene (Figure 5a), the electrons and holes diffuse in opposite directions to equate Fermi levels, causing depletion layer formation and energy band bending (Figure 5b). In the air environment, oxygen molecules adsorbed on ZnO accept electrons from its conduction band to form oxygen

https://doi.org/10.1021/acsmeasuresciau.1c00043
ACS Meas. Sci. Au 2022, 2, 113−119

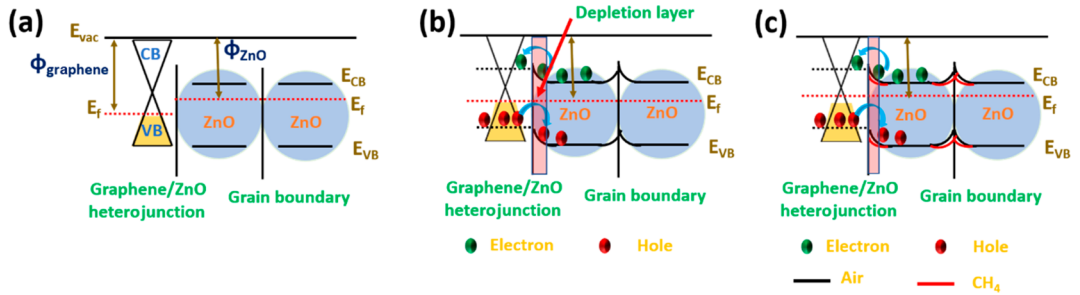

Figure 5. Sensing mechanism of GZnO to CH_4 gas: (a) work functions and energy bands of ZnO and graphene before contact, (b) Fermi level alignment and depletion layer formation after contact in air, and (c) Fermi level shift and variation in depletion layer width after exposure to CH_4 ($\Phi_{graphene}$: work function of graphene, Φ_{ZnO}: work function of ZnO, CB: conduction band, VB: valence band, E_{CB}: conduction band minimum, E_{VB}: valence band minimum energy, E_F: Fermi level).

ions. It leads to an increase in depletion width and potential barrier height at p−n junctions between graphene. In addition, the grain boundary potential barrier height increases with extracting electrons from ZnO by adsorbed oxygen molecules. It leads to an increase in sensor resistance as the potential barriers and depletion layers oppose the flow of charge carriers. Upon exposure to CH_4, the adsorbed gas molecules react with oxygen ions at grain boundaries and p−n junctions and release the electrons back to the conduction band. Thus, the depletion width and potential barrier heights are reduced (Figure 5c), and consequently, the sensor's resistance decreases.

The response time measured above is acceptable for most practical applications. However, some applications demand that the target gas concentration be measured within a few seconds. Thus, the measurement time should be decreased to use this sensor in such applications. The diffusion of gas molecules through the sensing layer and their immobilization at adsorption sites can be described using (4)[26]

$$\frac{\partial C}{\partial t} = D\frac{\partial^2 C}{\partial x^2} - \frac{\partial N}{\partial t} \tag{4}$$

where C is the gas concentration, D is the diffusion coefficient of the gas through the sensing layer, N is the number of molecules immobilized at adsorption sites, x is the depth from the surface of the sensing layer, and t is the time. Assuming N_0 is the total number of available adsorption sites in the film, the site coverage (θ) can be represented with (5), and the reaction kinetics can be represented with the Elovich equation (6)

$$\theta = \frac{N}{N_0} \tag{5}$$

$$\frac{\partial \theta}{\partial t} = a\exp(-b\theta) \tag{6}$$

where a and b are constants. The analytical solution to the diffusion equation can be discussed in terms of two limiting cases.

Case 1: Diffusion Limited Process

In this case, the diffusion process is much slower compared to the reaction kinetics, and the time required for the sensing process depends only on gas diffusion through the sensing layer. The immobilized gas molecules at the adsorption site can be written as (7)

$$N = N_0 K C^r \tag{7}$$

where K is the adsorption coefficient. For linear gas sensors, $r = 1$, and the concentration as a function of depth and time can be written as (8)[26,27]

$$\frac{C(x,t)}{C_0} = 1 - \frac{4}{\pi}\sum_{i=0}^{\infty}\frac{(-1)^i}{(i+0.5)}\exp\left(\frac{-(i+0.5)^2\pi^2 D_e t}{x_0^2}\right)\cos\left(\frac{(i+0.5)\pi x}{x_0}\right) \tag{8}$$

where $D_e = \frac{D}{1+KN_0}$ is the effective diffusion constant, and x_0 is the thickness of the sensing layer. The total number of molecules immobilized at the adsorption sites is directly proportional to the concentration, which depends only on the time t and effective diffusion constant D_e. The effective diffusion constant depends on the total number of adsorption sites and adsorption coefficient, constants for a given material, and the gas. Therefore, the response remains the same at a particular time for the repeated exposures of the same concentration of the target gas.

Case 2: Reaction Limited Process

In this case, diffusion is instantaneous compared to adsorption kinetics. In such cases, the concentration at any point is independent of time. Then, the site occupancy with time can be written as (9).[28−30]

$$\theta(t) = \frac{1}{b}\ln(abt + 1) \tag{9}$$

The above equation can deduce that the number of molecules immobilized at the adsorption site depends only on time and is constant at a particular time. Therefore, the response at a particular time depends only on the number of adsorbed molecules, which is directly proportional to the gas concentration.

The second-order reversible reaction and corresponding adsorption−desorption kinetics of the gas sensor is given by (10) and (11), respectively

$$c_R + c_A \underset{\beta}{\overset{\alpha}{\rightleftharpoons}} c_{RA} \tag{10}$$

$$\frac{dc_{RA}(t)}{dt} = \alpha c_R(t)c_A(t) - \beta c_{RA}(t) \tag{11}$$

where α is the rate of the forward reaction, β is the rate of the backward reaction, c_A is the concentration of the analyte, c_R is the reversible binding site concentration, and c_{RA} is the analyte concentration bounded on reversible binding sites.[31] By applying the initial condition $C_{RA}(t) = 0$, we get the solution as in (12)

https://doi.org/10.1021/acsmeasuresciau.1c00043
ACS Meas. Sci. Au 2022, 2, 113−119

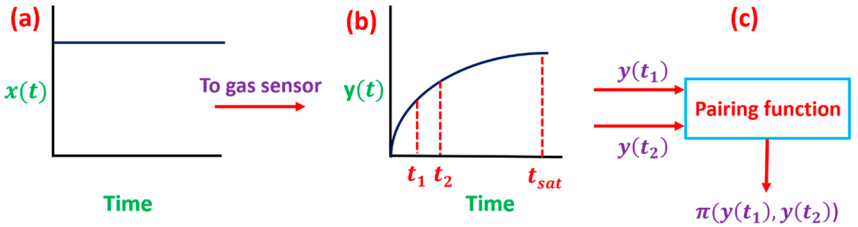

Figure 6. Pairing the gas concentration to a unique number to reduce the measurement time: (a) step input corresponding to gas concentration, (b) transient response of the sensor, and (c) pairing two temporal responses with a unique pairing number using a pairing function.

$$c(t) = k[1 - e^{-(\alpha c_A + \beta)t}] \tag{12}$$

$$\text{As } \frac{R}{R_0} \propto c(t)$$

$$\frac{R}{R_0} = k_1[1 - e^{-k_2 t}] \tag{13}$$

where $k_1 = k$ and $k_2 = (\alpha c_A + \beta)$ are constants. The exponential fit of the transient response in Figure S3 with a coefficient of determination close to unity agrees with the above assumption.

From the above analysis, we concluded that the temporal response is constant at a specific time after exposure of the target gas with the same concentration. However, two different concentrations may have the same response at a particular time, as shown in Figure S4 containing two exponential plots intersecting each other. Thus, we considered two different times to measure the response of the sensors and mapped the two responses to a unique pairing number, as shown in Figure 6. We considered the input as a step function and the response as an exponential function as represented in Figure 6a and Figure 6b, respectively. As no two exponential plots may coincide at two points on the time axis (t_1 = 20 s and t_2 = 30 s), the combination of corresponding temporal responses ($y(t_1)$ and $y(t_2)$) can be used to measure the concentration. As we have two temporal response values, we cannot directly fit the response as a function of concentration. Thus, we used the Cantor pairing function (Figure 6c) to map the two temporal response values to a single integer value. The pairing function is a process of encoding two natural numbers into a unique natural number. However, the response values are not integers to be used for cantor pairing. To resolve it, we made the response an integer value by multiplying the response of GZnO with 10 and subtracting the result with 10. The pairing number of modified response values is achieved with the Cantor pairing function in (14)

$$\pi(y(t_1), y(t_2)) = \frac{1}{2}(y(t_1) + y(t_2))(y(t_1) + y(t_2) + 1) + y(t_2) \tag{14}$$

where π is the pairing function of two integers, $y(t_1)$ and $y(t_2)$. In this case, $y(t_1)$ and $y(t_2)$ are the modified relative temporal response (10(temporal response)-10) values at two different time intervals t_1 and t_2, for a given concentration of the exposed gas. Figure 7 shows the calibration graph, representing the average pairing number of 3 responses as a function of the target gas concentration, and Table S1 shows the corresponding mean and standard deviation values. It can be observed that the maximum error in predicting the concentration from the transient response is 10.74%, which is acceptable in most gas sensing applications. The GZnO sensor can quantify the methane concentration in just 30 s. The average pairing number of 3 devices is the nonlinear power function given by (15)

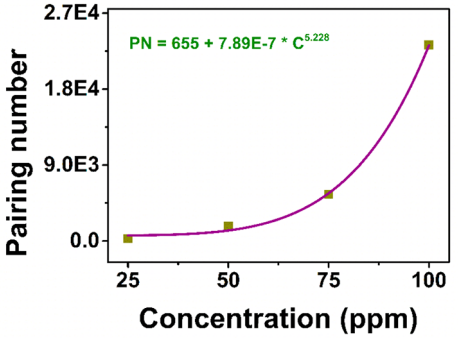

Figure 7. Average pairing number of the transient response as a function of the concentration of CH_4.

$$PN = 655 + 7.89E - 7{*}C^{5.228} \tag{15}$$

Like a steady-state response, the pairing number associated with the transient response also has power-law relation with the gas concentration. Therefore, the target gas can be detected and quantified within 30 s using the proposed sensor with the transient analysis. Unlike the existing algorithms, it is a computationally less intensive approach and can be helpful to monitor target gases in remote locations where low-power rapid sensing technology is required.

4. CONCLUSION

In summary, we described an analytical method to reduce the measurement time of the CH_4 concentration with a chemiresistive gas sensor. In this method, the temporal responses at two different fixed times, 20 and 30 s, were measured after the sensor's exposure to the target gas and mapped to a unique pairing number. The pairing number exhibits a power-law relation with the gas concentration, and thus, the target gas concentration can be quantified in just 30 s irrespective of the response time. As the proposed approach does not involve any computationally intensive algorithms, it can be used in the applications in which the gas concentration should be measured in a few seconds with the least possible resources. Though this technique is demonstrated with a gas sensor, it can be utilized in many other chemical sensors such as biosensors and humidity sensors, where relatively fast measurements are necessary.

■ ASSOCIATED CONTENT

Supporting Information

The Supporting Information is available free of charge at https://pubs.acs.org/doi/10.1021/acsmeasuresciau.1c00043.

Figures of schematic of gas sensing setup, sensor's response as a function of sensing layer thickness, exponential fitting of transient response, and two

https://doi.org/10.1021/acsmeasuresciau.1c00043
ACS Meas. Sci. Au 2022, 2, 113−119

exponential response curves intersecting at one point and table of average and standard deviation of pairing numbers (PDF)

AUTHOR INFORMATION

Corresponding Author

Shiv Govind Singh − *Department of Electrical Engineering, Indian Institute of Technology Hyderabad, Kandi 502285, India;* orcid.org/0000-0001-7319-879X; Phone: 040-2302-6076; Email: sgsingh@ee.iith.ac.in; Fax: 040-2301-6032

Author

Srinivasulu Kanaparthi − *Department of Electrical Engineering, Indian Institute of Technology Hyderabad, Kandi 502285, India*

Complete contact information is available at: https://pubs.acs.org/10.1021/acsmeasuresciau.1c00043

Funding

This research is supported by the Department of Biotechnology, under the Ministry of Science and Technology, India (Grant Number: BT/PR22239/NNT/28/1269/2017).

Notes

The authors declare no competing financial interest.

ACKNOWLEDGMENTS

S.K. acknowledges the Ministry of Education (MoE), India, for financial assistance.

REFERENCES

(1) Mamun, M. A. Al; Yuce, M. R. Recent Progress in Nanomaterial Enabled Chemical Sensors for Wearable Environmental Monitoring Applications. *Adv. Funct. Mater.* **2020**, *30* (51), 2005703.

(2) John, A. T.; Murugappan, K.; Nisbet, D. R.; Tricoli, A. An Outlook of Recent Advances in Chemiresistive Sensor-Based Electronic Nose Systems for Food Quality and Environmental Monitoring. *Sensors* **2021**, *21* (7), 2271.

(3) Aggas, J. R.; Sánchez-Sinencio, E.; Guiseppi-Elie, A. Wien Oscillator Using Organic Enzyme-Chemiresistors for Fused Measurement of Glucose and Lactate. *Adv. Intell. Syst.* **2020**, *2* (7), 2000004.

(4) Li, S.; Chiu, C. A Smart Pillow for Health Sensing System Based on Temperature and Humidity Sensors. *Sensors* **2018**, *18* (11), 3664.

(5) Kanaparthi, S.; Singh, S. G. Discrimination of Gases with a Single Chemiresistive Multi-Gas Sensor Using Temperature Sweeping and Machine Learning. *Sens. Actuators, B* **2021**, *348*, 130725.

(6) Kanaparthi, S.; Singh, S. G. Drift Independent Discrimination of H_2S from Other Interfering Gases with a Metal Oxide Gas Sensor Using Extracted Adsorption-Desorption Noise. *Sens. Actuators, B* **2021**, *344*, 130146.

(7) Fahad, H. M.; Shiraki, H.; Amani, M.; Zhang, C.; Hebbar, V. S.; Gao, W.; Ota, H.; Hettick, M.; Kiriya, D.; Chen, Y.-Z.; Chueh, Y.-L.; Javey, A. Room Temperature Multiplexed Gas Sensing Using Chemical-Sensitive 3.5 nm Thin Silicon Transistors. *Sci. Adv.* **2017**, *3* (3), e1602557.

(8) Kanaparthi, S.; Singh, S. G. Chemiresistive Sensor Based on Zinc Oxide Nanoflakes for CO2 Detection. *ACS Appl. Nano Mater.* **2019**, *2* (2), 700−706.

(9) Pan, X.; Zhao, X.; Chen, J.; Bermak, A.; Fan, Z. A Fast-Response/Recovery ZnO Hierarchical Nanostructure Based Gas Sensor with Ultra-High Room-Temperature Output Response. *Sens. Actuators, B* **2015**, *206*, 764−771.

(10) Zhihua, L.; Xucheng, Z.; Jiyong, S.; Xiaobo, Z.; Xiaowei, H.; Tahir, H. E.; Holmes, M. Fast Response Ammonia Sensor Based on Porous Thin Film of Polyaniline/Sulfonated Nickel Phthalocyanine Composites. *Sens. Actuators, B* **2016**, *226*, 553−562.

(11) Osorio-Arrieta, D. L.; Muñoz-Mata, J. L.; Beltrán-Pérez, G.; Castillo-Mixcóatl, J.; Mendoza-Barrera, C. O.; Altuzar-Aguilar, V.; Muñoz-Aguirre, S. Reduction of the Measurement Time by the Prediction of the Steady-State Response for Quartz Crystal Microbalance Gas Sensors. *Sensors* **2018**, *18* (8), 2475.

(12) Muezzinoglu, M. K.; Vergara, A.; Huerta, R.; Rulkov, N.; Rabinovich, M. I.; Selverston, A.; Abarbanel, H. D. I. Acceleration of Chemo-Sensory Information Processing Using Transient Features. *Sens. Actuators, B* **2009**, *137* (2), 507−512.

(13) Burgués, J.; Marco, S. Wind-Independent Estimation of Gas Source Distance From Transient Features of Metal Oxide Sensor Signals. *IEEE Access* **2019**, *7*, 140460−140469.

(14) Castillo, E.; Salmerón, J. F.; Falco, A.; Loghin, F. C.; Romero, F. J.; Lugli, P.; Morales, D. P.; Rivadeneyra, A. An Optimized Measurement Algorithm for Gas Sensors Based on Carbon Nanotubes: Optimizing Sensor Performance and Hardware Resources. *IEEE Internet Things J.* **2019**, *6* (5), 9140−9146.

(15) Siadat, M.; Losson, E.; Ahmadou, D.; Lumbreras, M. Detection Optimization Using a Transient Feature from a Metal Oxide Gas Sensor Array. *Sensors & Transducers* **2014**, *27*, 340−346.

(16) Zhang, Q.; Li, S.; Tang, W.; Guo, X. Fast Measurement With Chemical Sensors Based on Sliding Window Sampling and Mixed-Feature Extraction. *IEEE Sens. J.* **2020**, *20* (15), 8740−8745.

(17) Čulic Gambiroža, J.; Mastelić, T.; Kovačević, T.; Čagalj, M. Predicting Low-Cost Gas Sensor Readings From Transients Using Long Short-Term Memory Neural Networks. *IEEE Internet Things J.* **2020**, *7* (9), 8451−8461.

(18) Fonollosa, J.; Sheik, S.; Huerta, R.; Marco, S. Reservoir Computing Compensates Slow Response of Chemosensor Arrays Exposed to Fast Varying Gas Concentrations in Continuous Monitoring. *Sens. Actuators, B* **2015**, *215*, 618−629.

(19) Kanaparthi, S.; Singh, S. G. Solvent-Free Fabrication of a Room Temperature Ammonia Gas Sensor by Frictional Deposition of a Conducting Polymer on Paper. *Org. Electron.* **2019**, *68*, 108−112.

(20) Kanaparthi, S.; Kayal, S.; Singh, S. G. Simple and Facile Microfabrication of a Flexible Interdigitated Capacitor for Sensing Applications. *Flex. Print. Electron.* **2019**, *4* (1), 015005.

(21) da Silva, E. T. S. G.; Alves, T. M. R.; Kubota, L. T. Direct Toner Printing: A Versatile Technology for Easy Fabrication of Flexible Miniaturized Electrodes. *Electroanalysis* **2018**, *30* (2), 345−352.

(22) Tang, X.; Jan, S. S.; Qian, Y.; Xia, H.; Ni, J.; Savilov, S. V.; Aldoshin, S. M. Graphene Wrapped Ordered $LiNi_{0.5}Mn_{1.5}O_4$ Nanorods as Promising Cathode Material for Lithium-Ion Batteries. *Sci. Rep.* **2015**, *5*, 11958.

(23) Hezarjaribi, S. T.; Nasirian, S. An Enhanced Fast Ethanol Sensor Based on Zinc Oxide/Nickel Oxide Nanocomposite in Dynamic Situations. *J. Inorg. Organomet. Polym. Mater.* **2020**, *30*, 4072−4081.

(24) Sinha, M.; Mahapatra, R.; Mondal, B.; Maruyama, T.; Ghosh, R. Ultrafast and Reversible Gas-Sensing Properties of ZnO Nanowire Arrays Grown by Hydrothermal Technique. *J. Phys. Chem. C* **2016**, *120*, 3019−3025.

(25) Dang, T. K.; Son, N. T.; Lanh, N. T.; Phuoc, P. H.; Viet, N. N.; Thong, L. V.; Hung, C. M.; Duy, N. V.; Hoa, N. D.; Hieu, N. V. Extraordinary H2S Gas Sensing Performance of ZnO/RGO External and Internal Heterojunctions. *J. Alloys Compd.* **2021**, *879*, 160457.

(26) Gardner, J. W.; Iskandarani, M. Z.; Bott, B. Effect of Electrode Geometry on Gas Sensitivity of Lead Phthalocyanine Thin Films. *Sens. Actuators, B* **1992**, *9* (2), 133−142.

(27) Gardner, J. W. A Non-Linear Diffusion-Reaction Model of Electrical Conduction in Semiconductor Gas Sensors. *Sens. Actuators, B* **1990**, *1* (1), 166−170.

(28) Ho, K.-C.; Tsou, Y.-H. Chemiresistor-Type NO Gas Sensor Based on Nickel Phthalocyanine Thin Films. *Sens. Actuators, B* **2001**, *77* (1), 253−259.

(29) Aharoni, C.; Tompkins, F. C. Kinetics of Adsorption and Desorption and the Elovich Equation. In *Advances in Catalysis*; Eley,

D. D., Pines, H., Weisz, P. B., Eds.; Academic Press: 1970; Vol. *21*, pp 1−49, DOI: 10.1016/S0360-0564(08)60563-5.
(30) Altındal, A.; Kurt, Ö.; Şengül, A.; Bekaroğlu, Ö Kinetics of CO2 Adsorption on Ball-Type Dicopper Phthalocyanine Thin Film. *Sens. Actuators, B* **2014**, *202*, 373−381.
(31) Mackin, C.; Schroeder, V.; Zurutuza, A.; Su, C.; Kong, J.; Swager, T. M.; Palacios, T. Chemiresistive Graphene Sensors for Ammonia Detection. *ACS Appl. Mater. Interfaces* **2018**, *10*, 16169−16176.

https://doi.org/10.1021/acsmeasuresciau.1c00043
ACS Meas. Sci. Au 2022, 2, 113−119